Eur. Phys. J. Special Topics **217**, 91–102 (2013)

DOI: 10.1140/epjst/e2013-01758-6

THE EUROPEAN PHYSICAL JOURNAL SPECIAL TOPICS

Regular Article

Tailoring Anderson localization by disorder correlations in 1D speckle potentials

Marie Piraud and Laurent Sanchez-Palencia

Laboratoire Charles Fabry, Institut d'Optique, CNRS, Univ. Paris Sud,
2 avenue Augustin Fresnel, 91127 Palaiseau Cedex, France

Received 7 September 2012 / Received in final form 15 January 2013
Published online 11 March 2013

Abstract. We study Anderson localization of single particles in continuous, correlated, one-dimensional disordered potentials. We show that tailored correlations can completely change the energy-dependence of the localization length. By considering two suitable models of disorder, we explicitly show that disorder correlations can lead to a nonmonotonic behavior of the localization length versus energy. Numerical calculations performed within the transfer-matrix approach and analytical calculations performed within the phase formalism up to order three show excellent agreement and demonstrate the effect. We finally show how the nonmonotonic behavior of the localization length with energy can be observed using expanding ultracold-atom gases.

1 Introduction

Coherent transport in disordered media shows considerable interest in condensed-matter physics, with applications to normal solids [20,29], superconductors [10] and superfluids [38]. Coherent process can lead to the spatial localization of wave functions as a result of a subtle interference effect between multiple scattering paths, which survives disorder averaging. This effect, known as Anderson localization (AL), was first predicted for electronic matter waves [1]. It was later shown to be a universal phenomenon in wave physics [22], which permitted the first evidence of AL of classical waves [18,28,44,48,49]. The observation of AL in ultracold gases in one (1D) [5,39] and three (3D) [21,24] dimensions has triggered a renewed interest on matter wave localization [35,36], and paves the way to further investigation of many open questions [43].

Correlated disorder makes AL fascinatingly rich. Disorder correlations can change the localization properties, not only quantitatively but also qualitatively. For instance, disorder correlations with a finite support in momentum space were shown to induce effective mobility edges in 1D disorder [19,41,42], which was used to create materials with alternating localizing and almost transparent frequency windows [27], to enhance localization in microwave systems [26], and to propose realization of atomic band-pass filters [37]. Such correlations are also responsible for algebraic localization of matter waves with broad energy distributions [5,33,42]. It was also shown that in certain models of disorder with infinite-range correlations (i.e. such that the correlation function does not decay to zero at infinite distance) [12,25] or dimer-like

correlations [45,46], multiple localization-delocalization transition points can appear. Interestingly, tailoring the disorder correlations can lead to a counter-intuitive behavior of the energy dependence of the localization strength [34]. It can serve to discriminate quantum versus classical localization of particles, which is of particular interest for ultracold atoms where disordered potentials can be controlled [9,47].

The latter effect is the subject of the present paper. For the sake of clarity, consider matter waves in free space and subjected to a 1D disordered potential. The macroscopic behavior of AL is intimately related to the microscopic properties of single scattering from the asperities of the disorder. This shows up in the strong dependence of the localization length $L_{\rm loc}(E)$ – i.e. the characteristic length scale of exponential decay of localized wavefunctions – on the energy E and the Fourier component of the disordered potential V at twice the typical particle wave vector, $k_E \equiv \sqrt{2mE/\hbar}$: The 1D localization of a particle is dominated by the interference of quantum paths that are backscattered twice in the disorder with the forward propagating one. For weak disorder, the leading term is $L_{\rm loc}(E)^{-1} \propto \tilde{C}_2(2k_E)/E$, where $\tilde{C}_2$ is the structure factor (correlation function of the disordered potential in Fourier space, see below) [30]. For most models of disorder (e.g. for δ-correlated, Gaussian-correlated or usual speckle [9] disorder), $\tilde{C}_2$ is a constant or decreasing function, so that $L_{\rm loc}(E)$ is an increasing function of the particle energy E, which finds an intuitive interpretation as the higher energy the weaker localization.

Structured disorder correlations can however completely change the picture. If the disordered potential exhibits structures on a length scale of the order of k_E^{-1}, the scattering might not strictly increase with energy[1], and $L_{\rm loc}(E)$ can counter-intuitively decrease for increasing E [34]. In this work, we study this effect for particles in continuous disordered potentials with tailored correlations in one dimension. We first calculate the localization of the single-particle eigenstates, using both numerical calculations, based on the transfer-matrix approach, and the so-called *phase formalism*, which is well suited for perturbative expansion in 1D transmission schemes for a matterwave of fixed energy. Lowest-order analytical calculations reproduce the main physics and allow design of disorder correlations to realize the desired effect [34]. We study two alternative possibilities, which require only slight modifications of existing experimental schemes [5,7,8,11]. These calculations however show significant deviations with numerical data, but we show that they are quantitatively accounted for by next-order calculations. We finally discuss how to observe the nonmonotonic behavior of the localization length with energy with expanding ultracold-atom gases, and explicitly show that standard schemes should be adapted.

2 Tailoring disorder correlations in speckle potentials

Disorder realized by optical speckle [9,15,47] is relatively easy to obtain and its statistical properties are –to some extent– controllable, hence making a good candidate for tailoring correlations. Such disordered potentials have been used in several experiments to investigate the effect of disorder in ultracold-atom systems [5,7,8,11,21,24]. A 1D speckle pattern [15] is obtained by shining a coherent light beam onto an elongated aperture with a ground-glass plate diffuser, and observing the diffraction pattern that is created, for example in the focal plane of a lens (see Fig. 1). The role of the diffuser is mainly to imprint a random phase on the electric field at each point of its aperture. It follows from direct application of the laws of diffraction, that the electric field at a point z on the focal plane, $\mathcal{E}(z)$, is the sum of many complex

[1] This effect is similar to the well-known example of single scattering from double barriers (see for instance Ref. [2]).

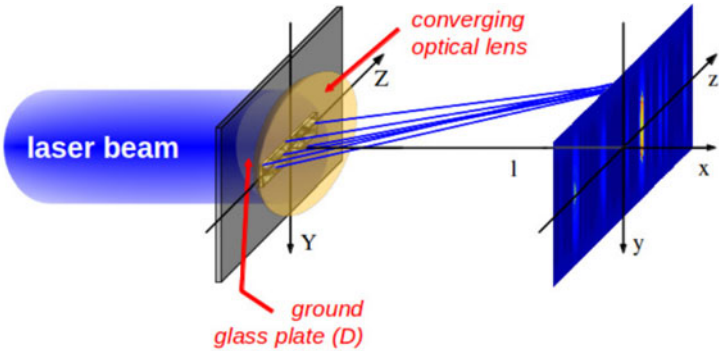

Fig. 1. Optical scheme to create a speckle pattern: A laser beam is diffracted by a ground-glass plate diffuser (D) with a 1D slit of pupil function $I_{\rm D}(Z)$, where Z spans the diffuser. The latter imprints a random phase on the various light paths. The intensity field, $\mathcal{I}(z)$, observed in the focal plane of a converging lens, is a speckle pattern, which creates a disordered potential $V(z)$ for the atoms.

independent random variables that corresponds to the components originating from every point of the plate and interfering in z. It is then a complex Gaussian random variable. In ultracold atom experiments, the atoms are sensitive to the light intensity, proportional to $|\mathcal{E}(z)|^2$. More precisely the atoms experience a potential that can be written $V(z) = V_{\rm R}[|\mathcal{E}(z)|^2/\overline{|\mathcal{E}|^2} - 1]$, so that $\overline{V} = 0$ and $\overline{V^2} = V_{\rm R}^2$ [9,47]. The amplitude of the disorder, $V_{\rm R}$, can be positive (so called 'blue detuned speckle') or negative ('red detuned speckle'), depending on the sign of the difference of the atom and laser frequencies. More generally, all statistical properties of the disordered potential $V(z)$ follow from basic laws of optics. For instance, one can show that the Fourier transform of the autocorrelation function of the potential is the auto-convolution of the pupil function $I_{\rm D}$. (intensity pattern exiting the diffuser):

$$\tilde{C}_2(k) \propto \int dZ\, I_{\rm D}\left(Z - \frac{\lambda_0 l}{4\pi}k\right) I_{\rm D}\left(Z + \frac{\lambda_0 l}{4\pi}k\right), \tag{1}$$

where λ_0 is the laser wavelength and l is the focal length [15]. For a thin slit of length $2R$ uniformly lit, which is the usual manner to obtain a speckle, we have $I_{\rm D}(Z) = I_0\Theta(R - |Z|)$, with Θ the Heaviside function [$\Theta(x) = 1$ if $x > 0$ and 0 otherwise], and we find[2]

$$\tilde{C}_2(k) = \pi V_{\rm R}^2 \sigma_{\rm R}\,[1 - |k|\sigma_{\rm R}/2]_{\oplus}\,, \tag{2}$$

where $[x]_{\oplus} = x\Theta(x)$ and $\sigma_{\rm R} = \lambda_0 l/2\pi R$ is the disorder correlation length. Therefore, the power spectrum of the speckle pattern is strictly decreasing with k. Note that this model has a cut-off in the Fourier components at $k_{\rm C} = 2\sigma_{\rm R}^{-1}$. This is a characteristics of speckle potentials, which in particular leads to the existence of effective mobility edges, as discussed in Refs. [17,31,41,42].

Modifying the pupil function $I_{\rm D}(Z)$ (i.e. changing the aperture of the diffusive plate or the spatial profile of the incident beam) allows us to tailor the disorder correlations [34,37]. In this work, we consider two configurations. In the first configuration, we propose to put a mask of width $2r$ at the center of the aperture, creating a double-slit. When doing so, a gap is created in the pupil function

[2] We use the conventions $\tilde{f}(\kappa) = \int f(u)e^{-i\kappa u}du$.

$[I_{\rm D}(Z) = I_0\Theta(|Z| - r)\Theta(R - |Z|)]$, leading, for $\rho = r/R > 0$, to an increase of the integral (1) on a certain interval of k, which is all the more marked that ρ is large:

$$\tilde{C}_2(k) = \frac{\pi V_{\rm R}^2 \sigma_{\rm R}}{(1-\rho)^2}\left\{ [1-\rho-|k|\sigma_{\rm R}]_\oplus + \frac{1}{2}[1-\rho-||k|\sigma_{\rm R}-(\rho+1)|]_\oplus \right\}. \tag{3}$$

In the second configuration, we propose to illuminate an infinitely-long slit by two mutually coherent Gaussian laser beams of waist w along Z and centered at $Z = \pm\Delta/2$. The two-point correlation function is then given by

$$\tilde{C}_2(k) = \frac{\sqrt{\pi} V_{\rm R}^2 \sigma_{\rm R}}{4}\left[{\rm e}^{-\frac{(k\sigma_{\rm R}-\kappa_0)^2}{4}} + 2{\rm e}^{-\frac{(k\sigma_{\rm R})^2}{4}} + {\rm e}^{-\frac{(k\sigma_{\rm R}+\kappa_0)^2}{4}} \right], \tag{4}$$

with $\sigma_{\rm R} = \lambda_0 l/\pi w$ and $\kappa_0 = 2\Delta/w$. For $\kappa_0 \gtrsim 3.7$, this function also increases on a certain interval of k. We will see in the following that the increase of $\tilde{C}_2(k)$ in both the double-slit and the double-Gaussian configurations can lead to an enhancement of localization with energy.

3 Anderson localization in 1D tailored speckle potentials

We now study AL of a single particle in these disordered potentials using the so-called phase formalism [30], which allows for efficient perturbative expansions [31]. Consider a particle of mass m and given energy E in the disordered potential. The corresponding eigenstate $\phi_E(z)$ is governed by the 1D Schrödinger equation

$$-(\hbar^2/2m)\partial_z^2\phi_E(z) + V(z)\phi_E(z) = E\phi_E(z). \tag{5}$$

Then, write the (real-valued) eigenfunction $\phi_E(z) = r(z)\sin[\theta(z)]$ and its spatial derivative $\partial_z\phi_E(z) = k_E r(z)\cos[\theta(z)]$. In this representation, Eq. (5) transforms into the set of equations

$$\partial_z\theta(z) = k_E\left(1 - \frac{V(z)}{E}\sin^2[\theta(z)]\right) \tag{6a}$$

$$\ln\left[\frac{r(z)}{r(0)}\right] = k_E\int_0^z dz'\frac{V(z')}{2E}\sin[2\theta(z')]. \tag{6b}$$

Equation (6a) can be solved in the form of a Born-like perturbative series for the phase θ in powers of the external potential V. Then, the Lyapunov exponent $\gamma(E) \equiv L_{\rm loc}(E)^{-1} \equiv \lim_{|z|\to\infty}\overline{\ln[r(z)]}/|z|$ can be calculated at each order in V by inserting the result of Eq. (6a) into Eq. (6b). It yields[3] $\gamma(E) = \sum_{n\geq 2}\gamma^{(n)}(E)$ with

$$\gamma^{(n)} = \frac{1}{\sigma_{\rm R}}\left(\frac{V_{\rm R}}{\sqrt{E}}\sqrt{\frac{2m\sigma_{\rm R}^2}{\hbar^2}}\right)^n f_n(k_E\sigma_{\rm R}), \tag{7}$$

where each function f_n depends on the n-point correlation function of the disorder, $C_n(z_1,...,z_{n-1}) = \overline{V(0)V(z_1)...V(z_{n-1})}$ [31]. In particular, the leading term of the series (Born approximation) is

$$f_2(\kappa) = \frac{1}{8}\frac{\tilde{C}_2(2\kappa/\sigma_{\rm R})}{V_{\rm R}^2\sigma_{\rm R}}\,. \tag{8}$$

[3] Note that the first-order term vanishes because $\overline{V} = 0$.

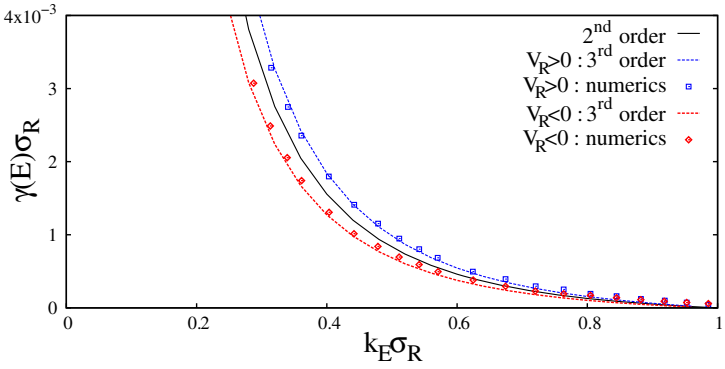

Fig. 2. Lyapunov exponent for both blue- and red-detuned speckles with the standard correlation function (2) and $V_{\mathrm{R}} = \pm 0.01625(\hbar^2/m\sigma_{\mathrm{R}}^2)$. Shown are the numerical results extracted from a transfer matrix method (space step of $\Delta z = 0.1\sigma_{\mathrm{R}}$ and total system size of $L_{\mathrm{tot}} = 411775\sigma_{\mathrm{R}}$ with random initial conditions) averaged over 5000 disorder realizations (blue squares: $V_{\mathrm{R}} > 0$, red diamonds: $V_{\mathrm{R}} < 0$), and analytical results obtained from the phase formalism up to order 2 (solid black line) and up to order 3 (dotted blue and red lines).

This term generally captures most localization properties in 1D disorder, in particular the effect of the tailored correlations we consider here. Previous work has however shown some discrepancies between analytic calculations in the Born approximation and numerical calculations [34]. Therefore, we will also include the next-order term [31]:

$$f_3(\kappa) = \frac{-1}{4}\int_{-\infty}^{0} du \int_{-\infty}^{u} dv \frac{C_3(u\sigma_{\mathrm{R}}, v\sigma_{\mathrm{R}})}{V_{\mathrm{R}}^3}\sin(2\kappa v). \tag{9}$$

In addition, we will perform numerical calculations for the transmission through the 1D disordered potential of a particle governed by Eq. (5), using transfer matrix techniques [32].

Let us start with the standard (single-slit) configuration where the pupil function is uniform and nonzero in the interval $-R < Z < +R$, which corresponds to the correlation function given by Eq. (2). Figure 2 shows the Lyapunov exponent in this configuration, for both blue- and red-detuned speckle potentials, with parameters relevant for current experiments [5]. The numerical data (blue squares and red diamonds) are averaged over 5000 realizations for each value of k_E. The analytic calculations of the Lyapunov exponent in the Born approximation [$\gamma^{(2)}(E)$ given by Eq. (7) with $n = 2$ and Eq. (8); solid black line], which do not depend on the sign of V_{R}, fairly reproduce the numerical data. In this standard configuration, both numerics and analytic calculation in the Born approximation confirm that the Lyapunov exponent, i.e. the localization strength, decreases with increasing particle energy, hence following the intuitive behavior. We however find a significant discrepancy, which depends on the sign of V_{R}, between the numerics and the analytics. A similar discrepancy was also observed in Ref. [34] but the numerics were not calculating $\gamma(E)$ in a direct way as in the present work. As is seen on Fig. 2, this discrepancy is very well accounted for by analytic calculations to the next order in the perturbative series, $\gamma^{(2)}(E) + \gamma^{(3)}(E)$, where $\gamma^{(3)}(E)$ is given by Eq. (7) with $n = 3$ and Eq. (A.1) with $\rho = 0$. Note that $\gamma^{(3)}$ depends on the sign of V_{R}.

Figure 2 shows the average values of the Lyapunov exponent, which we write $\overline{\gamma}(E)$ in this paragraph. For the sake of completeness, we show in Fig. 3 some distributions of the Lyapunov exponents $\gamma(E)$ obtained for the different realizations of the potential

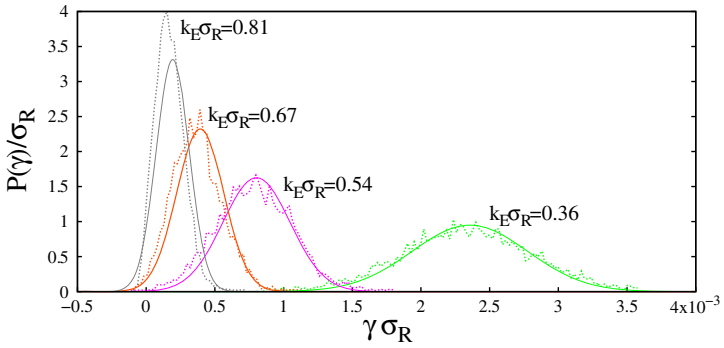

Fig. 3. Probability distributions of the Lyapunov exponents obtained by transfer matrix calculations (dotted lines) with the disorder parameters of Fig. 2, $V_R > 0$ (space step of $\Delta z = 0.1\sigma_R$ and total system size of $L_{tot} = 13333\sigma_R$ with random initial conditions), and various energies (indicated on the figure). The solid lines are the corresponding theoretical distributions (10).

at four values of the energy, together with the Gaussian distribution

$$P(\gamma) = \frac{1}{\sqrt{2\pi}\Delta_\gamma} \exp\left[-\frac{(\gamma-\overline{\gamma})^2}{2\Delta_\gamma^2}\right] \tag{10}$$

with $\Delta_\gamma = \sqrt{\overline{\gamma}/L_{tot}}$ and L_{tot} the system size, which is expected for δ-correlated disorder when $L_{tot} \gg 1/\overline{\gamma}$. For low energy, we find a good agreement. Since $\gamma(E) = -\ln(T)/2L_{tot}$, where T is the transmission probability of the wave through a sample of finite length L_{tot}, it shows that the transmission probability T follows a log-normal distribution also in the correlated disorder we are considering. At high energy ($k_E\sigma_R \gtrsim 0.8$) the numerical distributions differ from Eq. (10). This is expected because for $k_E\sigma_R = 0.81$, we find $1/\overline{\gamma} \sim 5000\sigma_R$, which is of the order of magnitude of $L_{tot} = 13333\sigma_R$.

As discussed above, for standard disorder, i.e. with a power spectrum $\tilde{C}_2$ that is a constant or decreasing function of k, the Lyapunov exponent $\gamma^{(2)}(E)$ decreases with the energy E. Let us now consider the double-slit configuration, of correlation function given by Eq. (3). Inserting the latter into Eq. (8), we find that, for $\rho > 0.25$, $\gamma^{(2)}(E)$ shows an increase in a certain interval of k, which is all the more pronounced that ρ approaches 1. This indicates that in those tailored potentials, $\gamma(E)$ can counter-intuitively increase with energy. In order to study this effect precisely, we performed numerical (transfer-matrix approach) and analytical (phase formalism approach) calculations for the considered tailored speckle potential with $\rho = 1/3$, as done for the standard speckle potential. The results of the numerical calculations (blue squares and red diamonds) and of analytical calculations up to order three in the phase formalism (dotted blue and red lines) are shown on Fig. 4. They confirm that, for both blue and red detunings, $\gamma(E)$ exhibits an increase with E for $k_E\sigma_R \in [0.35, 0.6]$. As for the standard speckle potential, the numerical results follow the trend of the 2nd order term in the phase formalism (solid black line in Fig. 4). The 3rd order term is given in the appendix [Eq. (A.1)]. For $k_E\sigma_R \in [0.4, 1]$, it accounts very well for the discrepancy between the numerics and the 2nd order term (solid black line). For low energy (i.e. $k_E\sigma_R \lesssim 0.4$), the 4th and higher order terms play a more important role, which is expected as we are approaching the limits of validity of the perturbative development.

In the above double-slit configuration, $\gamma(E)$ has a slope break near its maximum [see Eqs. (3), and (A.1) and Fig. 4], which is reminiscent of the sharp edges of the pupil

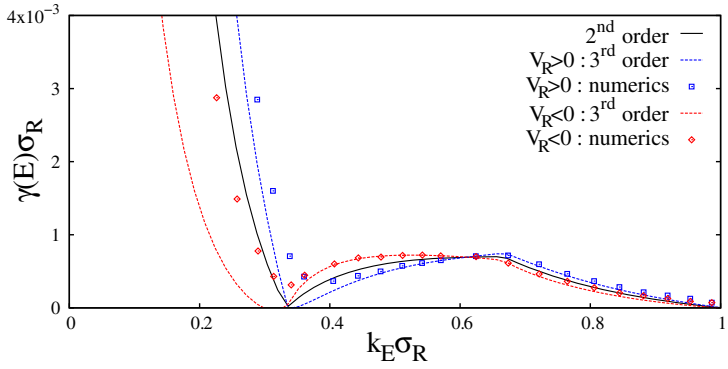

Fig. 4. Lyapunov exponent for speckles with the tailored correlation function (3) with $\rho = 1/3$, using the same methods and parameters as in Fig. 2. Blue squares: numerics with $V_{\mathrm{R}} > 0$; Red diamonds: numerics with $V_{\mathrm{R}} < 0$; Solid black line: order 2 in the phase formalism; Dotted blue and red lines: order 3 in the phase formalism.

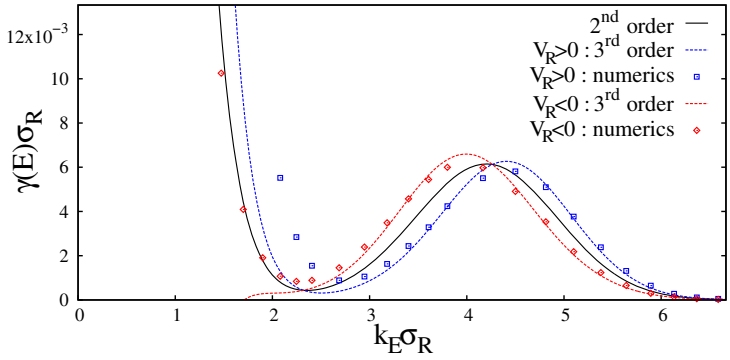

Fig. 5. Lyapunov exponent for speckles with the tailored correlation function (4) with $\kappa_0 = 8.88$ and $V_{\mathrm{R}} = \pm 0.72(\hbar^2/m\sigma_{\mathrm{R}}^2)$, using the same methods as in Figs. 2 and 4 (with a total system size of $L_{\mathrm{tot}} = 30880\sigma_{\mathrm{R}}$ and random initial conditions) averaged over 500 disorder realizations. Blue squares: numerics with $V_{\mathrm{R}} > 0$; Red diamonds: numerics with $V_{\mathrm{R}} < 0$; Solid black line: order 2 in the phase formalism; Dotted blue and red lines: order 3 in the phase formalism.

function. As it will presumably be inconvenient for experimental observations, we now consider the double-Gaussian configuration, which is obtained using two mutually coherent Gaussian beams shone onto an infinite diffusive plate, giving the power spectrum (4) [34]. For this configuration, $\gamma^{(2)}(E)$ shows an increase when $\kappa_0 \gtrsim 5.3$, which is all the more marked than κ_0 is large. In Fig. 5, we show the Lyapunov exponents obtained in this case for $\kappa_0 = 8.88$, with transfer matrices (blue squares and red diamonds) and with the phase formalism, up to order 2 (solid black line) and up to order 3 (dotted blue and red lines; see Eq. (A.2) in the appendix for the 3rd order term). In this configuration, we recover the same trend as in the other configuration, namely the Lyapunov exponent shows a significant increase in a given energy window, $k_E\sigma_{\mathrm{R}} \in [2.3, 4.2]$, the second order term, $\gamma^{(2)}(E)$, captures the main physics, and the discrepancy between the numerical results and $\gamma^{(2)}(E)$ are well accounted by the third order term, except at very low energy where the perturbative expansion breaks down. As expected, the behavior of $\gamma(E)$ is smoother for the double-Gaussian configuration compared to the double-slit configuration.

4 Observation scheme with ultracold atoms

In order to probe the nonmonotonous behavior of $\gamma(E)$ discussed above, one can use ultracold atoms, which proved a good means to observe 1D AL of matter waves with pseudo-periodic [39] and speckle [5] potentials. The preceding calculations of the Lyapunov exponent (a self-averaging quantity) directly apply to a 1D transmission scheme of a wave with fixed energy E. In ultracold-atom experiments [5,21,24,39] however, a matter-wavepacket with a broad energy distribution should be considered, and the measured quantity is the density profile obtained after releasing the atoms in the disorder, which is not directly related to the above calculations. The average stationary density of a noninteracting atomic gas, with initial negligible width, after evolution in the disorder reads [33,41,42] $n_\infty(z) = \int dE\ \mathcal{D}_{\rm E}(E) P_\infty(z|E)$, where $\mathcal{D}_{\rm E}(E)$ is the energy distribution of the atoms and

$$P_\infty(z|E) = \frac{\pi^2\gamma}{8}\int_0^\infty {\rm d}u\ u\,\sinh(\pi u)\left[\frac{1+u^2}{1+\cosh(\pi u)}\right]^2 \times \exp\{-(1+u^2)\gamma|z|/2\}\,, \tag{11}$$

with $\gamma = \gamma^{(2)}(E)$ given by Eqs. (7) and (8), is the probability of quantum diffusion calculated in the weak disorder approximation [3,13,14].

A first attempt to observe the nonmonotonous behavior of $\gamma(E)$ may be to consider the experimental scheme of Ref. [5]. In this case an interacting condensate is first produced in the Thomas-Fermi regime in a harmonic trap of frequency ω, and the trap is then switched-off at time $t = 0$. In a first stage the expansion of the atoms is driven by their interaction energy, and one can neglect the disordered potential. For $t \gg 1/\omega$, it produces an almost noninteracting gas with momentum distribution [6,23]

$$\mathcal{D}_{\rm i}(p) = (3/4p_{\rm cut})\left[1-(p/p_{\rm cut})^2\right]_\oplus\,. \tag{12}$$

We have performed numerical integration of the time-dependent Schrödinger equation for a particle with the initial momentum distribution (12) in the two-Gaussian tailored disordered potential with correlation function (4) and disorder parameters as in Fig. 5, for six realizations of the disordered potential [three with blue ($V_{\rm R} > 0$) and three with red ($V_{\rm R} < 0$) detuning][4]. After averaging the stationary density profiles over the six realizations, we fit $\ln[P_\infty(z)]$ as given by Eq. (11) to $\ln[\overline{n_\infty}(z)]$ with γ as the only fitting parameter[5]. The results, plotted on Fig. 6, show that the fitted Lyapunov exponent (black dots) slightly decreases with $k_{\rm cut}$ and saturates roughly beyond the minimum of the calculated $\gamma^{(2)}$. This is because the long distance behavior of $n_\infty(z)$ is dominated by the energy components with the largest localization lengths, i.e. those with the smallest $\gamma(E)$ [33,41,42]. Therefore this scheme does not enable us to probe the region where $\gamma(E)$ increases.

In order to observe the upturn of $\gamma(E)$, one can use an atomic energy distribution much narrower in energy and strongly peaked at a given $E_{\rm at}$, so that $n_\infty(z) \simeq P_\infty(z|E_{\rm at})$. As discussed in Ref. [34], it can be realized by either giving

[4] As in Refs. [33,34], we use a Crank-Nicolson algorithm with the following numerical parameters: space step $\Delta x = 0.03\sigma_{\rm R}$, time step $\Delta t = 1.1\hbar/E_{\sigma_{\rm R}}$, boxes of size $12\times10^3\sigma_{\rm R}$.

[5] The fits are performed in the space windows $-300\sigma_{\rm R} < z < -50\sigma_{\rm R}$ and $+50\sigma_{\rm R} < z < +300\sigma_{\rm R}$, corresponding to an experimentally accessible width of 1 mm for $\sigma_{\rm R} = 1.6\,\mu$m.

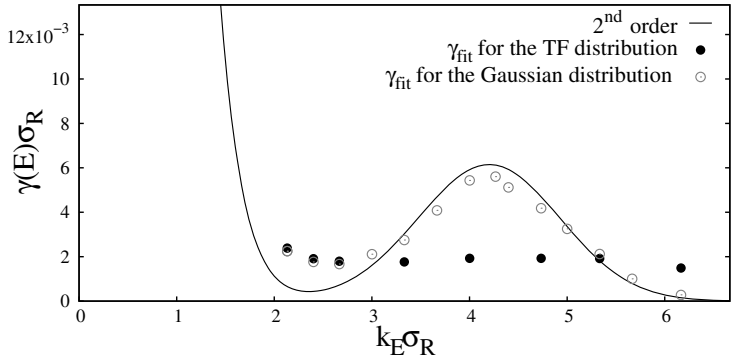

Fig. 6. Lyapunov exponent versus particle energy for speckles in the double-Gaussian configuration with $\kappa_0 = 8.88$ and $V_R = \pm 0.72(\hbar^2/m\sigma_R^2)$, obtained from Eq. (8) (solid black line) and from fits of Eq. (11) to the numerical data (points). The figure shows the values of γ_{fit} extracted from the average profile $\overline{n_\infty(z)}$, with initial Thomas-Fermi [TF, Eq. (12), full dots] and Gaussian [Eq. (13), open circles] momentum distributions.

a momentum kick to a noninteracting initially trapped gas or using an atom laser, both with a narrow energy width [4,16,40]. Using the momentum distribution

$$\mathcal{D}_i(p) = (1/\sqrt{2\pi}p_w)\exp\left[-(p-p_{at})^2/2p_w^2\right]. \tag{13}$$

with parameters relevant to current experiments, one can then extract the values of $\gamma(E_{at})$ by the same fitting procedure as above. The results, displayed on Fig. 6 (grey circles, reproduced from Fig. 2(a) of Ref. [34]), show a strong increase of $\gamma(E)$ as a function of k_{at}, which follows quite well Eq. (8). The scheme, which requires a small change in current experiments hence allows one to directly observe the nonmonotonic behavior of $\gamma(E)$ induced by the tailored correlations.

5 Conclusion

In summary, we have studied Anderson localization of noninteracting ultracold matterwaves in correlated disordered potentials. Tailoring of the disorder correlations can strongly affect the localization behavior, namely the localization length can increase with particle energy. Here we focused on the 1D case, providing more details compared to earlier works [34,37]. In particular, we show that although the Born approximation reproduces the overall behavior of the localization length, next-order terms are significant. We have found good agreement between exact numerical calculations and perturbation theory up to order three. We have compared two disorder configurations ('double-slit' and 'double-Gaussian') to realize the above effect. We finally discussed how to observe the effect with expanding ultracold atoms, explicitly showing that the scheme usually used in experiments [5,21,24,39] should be adapted.

We thank A. Aspect, Y. Castin, P. Chavel, D. Clément, and J.-J. Greffet for discussions. This research was supported by the European Research Council (FP7/2007-2013 Grant Agreement No. 256294), Agence Nationale de la Recherche (ANR-08-blan-0016-01), Ministère de l'Enseignement Supérieur et de la Recherche, Triangle de la Physique and Institut Francilien de Recherche sur les Atomes Froids (IFRAF). We acknowledge the use of the computing facility cluster GMPCS of the LUMAT federation (FR LUMAT 2764).

Appendix A. Third-order term in phase-formalism calculations

For the double-slit configuration, the f_3 function that intervenes in Eq. (7) reads

$$f_3(\kappa) = \frac{\pi}{8(1-\rho)^3}\left\{\Theta\left(\frac{1-\rho}{2}-\kappa\right) f_{3,1}(\kappa) + \Theta\left(\frac{1-\rho}{2}-\left|\kappa-\frac{\rho+1}{2}\right|\right) \times\left[\Theta\left(\kappa-\frac{\rho+1}{2}\right) f_{3,2}(\kappa)+\Theta\left(\frac{\rho+1}{2}-\kappa\right) f_{3,3}(\kappa)\right]\right\}, \tag{A.1}$$

with

$$f_{3,1}(\kappa) = g(2) - g[2(1-\kappa)] - 2g(2\kappa) + 2g(1-\rho) - g(2\rho) - 2g(1-\rho-2\kappa) + g(1-2\kappa+\rho) + g[2(\kappa+\rho)] - g(1+2\kappa+\rho),$$

$$f_{3,2}(\kappa) = -g(2\kappa) - g(1-\rho) + g(2\rho) + g(2\kappa+1-\rho) + g(2\kappa-2\rho) - g(1+\rho) + g(1-2\kappa+\rho),$$

and

$$f_{3,3}(\kappa) = g(2) - g[2(1-\kappa)] - g(2\kappa) + g(1-\rho) - g(-1+2\kappa-\rho) - g(1+\rho) + g(2\kappa-1-\rho)$$

where $g(x) \equiv x\ln(x)$.

For the double-Gaussian configuration, we find:

$$f_3(\kappa) = \frac{1}{32\sqrt{3}}\Bigg\{4\pi e^{-\frac{4}{3}\kappa^2}\operatorname{erfi}\left(\frac{\kappa}{\sqrt{3}}\right) + 2\pi e^{-\kappa^2}\times \tag{A.2}$$

$$\left[\left\{e^{-\frac{1}{3}(\kappa+\kappa_0)^2}\operatorname{erfi}\left(\frac{\kappa+\kappa_0}{\sqrt{3}}\right) + e^{-\frac{1}{3}(\kappa-\kappa_0)^2}\operatorname{erfi}\left(\frac{\kappa-\kappa_0}{\sqrt{3}}\right)\right\}\right.$$

$$+2e^{-\frac{\kappa_0^2}{4}}\cosh(\kappa\kappa_0)\left\{e^{-\frac{1}{3}(\kappa+\frac{\kappa_0}{2})^2}\operatorname{erfi}\left(\frac{\kappa+\kappa_0/2}{\sqrt{3}}\right)\right.$$

$$\left.\left.\left.+e^{-\frac{1}{3}(\kappa-\frac{\kappa_0}{2})^2}\operatorname{erfi}\left(\frac{\kappa-\kappa_0/2}{\sqrt{3}}\right)\right\}\right]\Bigg\}$$

where $\operatorname{erfi}(z) \equiv -i\operatorname{erf}(iz)$ is the imaginary error function, with $\operatorname{erf}(x) \equiv 2\int_0^x dt\, e^{-t^2}/\sqrt{\pi}$ the error function.

References

1. P.W. Anderson, Phys. Rev. **109**, 1492 (1958)
2. J.-L. Basdevant, J. Dalibard, *Quantum Mechanics* (Springer, Berlin, 2005)
3. V.L. Berezinskii, Sov. Phys. JETP **38**, 620 (1974)
4. A. Bernard, W. Guerin, J. Billy, F. Jendrzejewski, P. Cheinet, A. Aspect, V. Josse, P. Bouyer, New J. Phys. **13**, 065015 (2011)
5. J. Billy, V. Josse, Z. Zuo, A. Bernard, B. Hambrecht, P. Lugan, D. Clément, L. Sanchez-Palencia, P. Bouyer, A. Aspect, Nature (London) **453**, 891 (2008)
6. Y. Castin, R. Dum, Phys. Rev. Lett. **77**, 5315 (1996)

7. Y.P. Chen, J. Hitchcock, D. Dries, M. Junker, C. Welford, R.G. Hulet, Phys. Rev. A **77**, 033632 (2008)
8. D. Clément, P. Bouyer, A. Aspect, L. Sanchez-Palencia, Phys. Rev. A **77**, 033631 (2008)
9. D. Clément, A.F. Varón, J.A. Retter, L. Sanchez-Palencia, A. Aspect, P. Bouyer, New J. Phys. **8**, 165 (2006)
10. P.-G. de Gennes, *Superconductivity of Metals and Alloys* (Addison-Wesley, 1995)
11. D. Dries, S.E. Pollack, J.M. Hitchcock, R.G. Hulet, Phys. Rev. A **82**, 033603 (2010)
12. A.M. García-García, E. Cuevas, Phys. Rev. B **79**, 073104 (2009)
13. A.A. Gogolin, Sov. Phys. JETP **44**, 1003 (1976)
14. A.A. Gogolin, V.I. Mel'nikov, E.I. Rashba, Sov. Phys. JETP **42**, 168 (1976)
15. J.W. Goodman, *Speckle Phenomena in Optics: Theory and Applications* (Roberts and Co, Englewood, 2007)
16. W. Guerin, J.-F. Riou, J.P. Gaebler, V. Josse, P. Bouyer, A. Aspect, Phys. Rev. Lett. **97**, 200402 (2006)
17. E. Gurevich, O. Kenneth, Phys. Rev. A **79**, 063617 (2009)
18. H. Hu, A. Strybulevych, J.H. Page, S.E. Skipetrov, B.A. van Tiggelen, Nature Phys. **4**, 845 (2008)
19. F.M. Izrailev, A.A. Krokhin, Phys. Rev. Lett. **82**, 4062 (1999)
20. M. Janssen, Phys. Rep. **295**, 1 (1998)
21. F. Jendrzejewski, A. Bernard, K. Müller, P. Cheinet, V. Josse, M. Piraud, L. Pezzé, L. Sanchez-Palencia, A. Aspect, P. Bouyer, Nature Phys. **8**, 398 (2012)
22. S. John, Phys. Rev. Lett. **53**, 2169 (1984)
23. Yu. Kagan, E.L. Surkov, G.V. Shlyapnikov, Phys. Rev. A **54**, R1753 (1996)
24. S.S. Kondov, W.R. McGehee, J.J. Zirbel, B. DeMarco, Science **334**, 66 (2011)
25. S. Kotani, S. Taniguchi, Proc. Int. Symp. Kyoto (Mathematical Library, vol. 32, North-Holland, Amsterdam, 1984), p. 225
26. U. Kuhl, F.M. Izrailev, A.A. Krokhin, Phys. Rev. Lett. **100**, 126402 (2008)
27. U. Kuhl, F.M. Izrailev, A.A. Krokhin, H.-J. Stöckmann, Appl. Phys. Lett. **77**, 633 (2000)
28. Y. Lahini, A. Avidan, F. Pozzi, M. Sorel, R. Morandotti, D.N. Christodoulides, Y. Silberberg, Phys. Rev. Lett. **100**, 013906 (2008)
29. P.A. Lee, T.V. Ramakrishnan, Rev. Mod. Phys. **57**, 287 (1985)
30. I.M. Lifshits, S.A. Gredeskul, L.A. Pastur, *Introduction to the Theory of Disordered Systems* (Wiley, New York, 1988)
31. P. Lugan, A. Aspect, L. Sanchez-Palencia, D. Delande, B. Grémaud, C.A. Müller, C. Miniatura, Phys. Rev. A **80**, 023605 (2009)
32. C.A. Müller, D. Delande, *Ultracold Gases and Quantum Information*, edited by C. Miniatura et al., Lecture Notes of the Les Houches Summer School in Singapore 2009: vol. XCI, chapter Disorder and interference: localization phenomena (Oxford University Press, Oxford, 2011)
33. M. Piraud, P. Lugan, P. Bouyer, A. Aspect, L. Sanchez-Palencia, Phys. Rev. A **83**, 031603 (2011)
34. M. Piraud, A. Aspect, L. Sanchez-Palencia, Phys. Rev. A **85**, 063611 (2012)
35. M. Piraud, L. Pezzé, L. Sanchez-Palencia, Europhys. Lett. **99**, 50003 (2012)
36. M. Piraud, L. Pezzé, L. Sanchez-Palencia, Quantum transport of atomic matterwaves in anisotropic 2d and 3d disorder [`arXiv:1211.5872, 2012`]
37. M. Płodzień, S. Krzvsztof, Phys. Rev. A **84**, 023624 (2011)
38. J.D. Reppy, J. Low Temp. Phys. **87**, 205 (1992)
39. G. Roati, C. D'Errico, L. Fallani, M. Fattori, C. Fort, M. Zaccanti, G. Modugno, M. Modugno, M. Inguscio, Nature (London) **453**, 895 (2008)
40. N.P. Robins, C. Figl, S.A. Haine, A.K. Morrison, M. Jeppesen, J.J. Hope, J.D. Close, Phys. Rev. Lett. **96**, 140403 (2006)
41. L. Sanchez-Palencia, D. Clément, P. Lugan, P. Bouyer, A. Aspect, New J. Phys. **10**, 045019 (2008)
42. L. Sanchez-Palencia, D. Clément, P. Lugan, P. Bouyer, G.V. Shlyapnikov, A. Aspect, Phys. Rev. Lett. **98**, 210401 (2007)

43. L. Sanchez-Palencia, M. Lewenstein, Nature Phys. **6**, 87 (2010)
44. T. Schwartz, G. Bartal, S. Fishman, M. Segev, Nature (London) **446**, 52 (2007)
45. T.A. Sedrakyan, J.P. Kestner, S. Das Sarma, Phys. Rev. A **84**, 053621 (2011)
46. T. Sedrakyan, Phys. Rev. B **69**, 085109 (2004)
47. B. Shapiro, J. Phys. A: Math. Theor. **45**, 143001 (2012)
48. M. Störzer, P. Gross, C.M. Aegerter, G. Maret, Phys. Rev. Lett. **96**, 063904 (2006)
49. D.S. Wiersma, P. Bartolini, A. Lagendijk, R. Righini, Nature (London) **390**, 671 (1997)